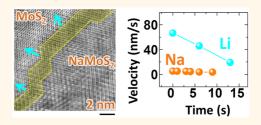# Atomic-Scale Probing of the Dynamics of Sodium Transport and Intercalation-Induced Phase Transformations in MoS$_2$

Peng Gao,*,[†] Liping Wang,[‡] Yuyang Zhang,[§] Yuan Huang,[⊥] and Kaihui Liu[†]

[†]School of Physics, Center for Nanochemistry, and Collaborative Innovation Center of Quantum Matter, Peking University, Beijing 100871, China, [‡]State Key Laboratory of Electronic Thin Films and Integrated Devices, University of Electronic Science and Technology of China, Chengdu 610054, China, [§]Beijing National Laboratory for Condensed Matter Physics and Institute of Physics, Chinese Academy of Sciences, Beijing 100190, China, and [⊥]Center for Functional Nanomaterials, Brookhaven National Laboratory, Upton, New York 11973, United States

ABSTRACT For alkali-metal-ion batteries, probing the dynamic processes of ion transport in electrodes is critical to gain insights into understanding how the electrode functions and thus how we can improve it. Here, by using *in situ* high-resolution transmission electron microscopy, we probe the dynamics of Na transport in MoS$_2$ nanostructures in real-time and compare the intercalation kinetics with previous lithium insertion. We find that Na intercalation follows the two-phase reaction mechanism, that is, trigonal prismatic 2H-MoS$_2$ → octahedral 1T-NaMoS$_2$, and the phase boundary is ~2 nm thick. The velocity of the phase boundary at <10 nm/s is 1 order smaller than that of lithium diffusion, suggesting sluggish kinetics for sodium intercalation. The newly formed 1T-NaMoS$_2$ contains a high density of defects and series superstructure domains with typical sizes of ~3−5 nm. Our results provide valuable insights into finding suitable Na electrode materials and understanding the properties of transition metal dichalcogenide MoS$_2$.

KEYWORDS: sodium-ion battery · *in situ* TEM · phase transition · molybdenum disulfide · transition metal dichalcogenide

Although lithium-ion batteries[1,2] (LIBs) have governed the current battery market for small portable electronic devices, for emerging large-scale applications, such as for electric vehicles and power grid storage,[3,4] concerns about limited natural abundance and uneven global distribution of lithium resources render the necessity to develop new battery systems other than LIBs. Among them, sodium-ion batteries (NIBs) are the leading candidates because of the large abundance and low cost of sodium. However, finding suitable materials as electrodes (both cathodes and anodes) is challenging for NIBs as sodium has a larger radius, that is, 55% larger than that of Li ions, and heavier mass, significantly impacting the ion transport and reaction kinetics within electrodes. As a result, many host materials which function well in LIBs, however, do not have enough space to allow reversible and rapid Na-ion insertion and extraction. For example, a layered graphite structure with a layer distance of 0.34 nm is the most commonly used anode in LIBs (LiC$_6$), but few Na ions can be inserted (~NaC$_{70}$ in ref 5).

Compared to graphite, transition metal dichalcogenides such as MoS$_2$ have a similar layered structure but can accommodate larger radius Na$^+$ (as well as Mg^{2+}, ref 6, and K$^+$, ref 7), making them promising candidates for sodium-ion battery electrode materials.[8−11] For example, MoS$_2$ and carbon nanosphere composite electrodes can maintain a capacity of 400 mAhg^{-1} for 300 cycles at a high current density of 1 C.[11] However, the structure framework of MoS$_2$ is sensitive to the alkali-metal-ion intercalation, which could induce a structure transition between trigonal 2H- and octahedral 1T-MoS$_2$ phases accompanied by a change in electronic states between semiconducting and metallic.[12−14] Such a transition of the structure framework and electronic structure, in turn, should significantly influence both the electrical and the ionic migration behavior during the alkali-metal-ion intercalation/extraction.[12−14] Therefore, the dynamics of alkali-metal-ion transport in the layered MoS$_2$ along with the structure transition are still largely unknown due to the strong coupling between structure and properties.[8,15]
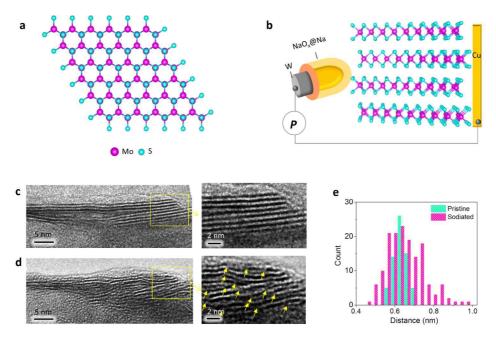
Figure 1. Tracking Na intercalation in MoS$_2$ nanosheets in real-time by *in situ* high-resolution TEM. Pristine MoS$_2$ nanosheet with the viewing direction of (a) [001] and (b) [100]. Schematic showing the battery cell used for *in situ* TEM measurements consisting of a MoS$_2$ nanosheet and metallic Na coated by a thin layer of NaO$_x$ acting as a solid-state electrolyte. (c) High-resolution TEM image from the edge of a pristine MoS$_2$ nanosheet. Right inset shows an enlarged view of the layered structure. (d) Same region after sodium insertion showing that the structure becomes defective. The yellow arrows in the right inset highlight the cracks of the layered structure. (e) Distribution of interlayer distances in the pristine and Na-intercalated MoS$_2$. In this plot, the mean value for the pristine state is normalized to 0.615 nm. The mean value for the sodium-intercalated state is measured to be 0.636 $\pm$ 0.097 nm.

Here, we use *in situ* high-resolution transmission electron microscopy to track the Na intercalation and structural evolution in MoS$_2$ nanostructures in real-time. Previous study of X-ray diffraction (XRD) and *ex situ* scanning transmission electron microscopy performed by Wang *et al.*[15] provides valuable insights into the global phase change, lattice expansion, and Na-ion coordination in MoS$_2$. Unlike the bulk-based techniques that collect information from large areas of agglomerates or *ex situ* techniques that involve inevitable sample variability in microstructures and potential contamination, *in situ* transmission electron microscopy (TEM) allows us to probe in real-time the phase nucleation, microstructure, and propagation of the phase boundary, the localized phase distribution, and the defect-mediated solid-state phase transformations in various functional materials down to the atomic scale.[16,17] Therefore, the *in situ* TEM study can give complementary information that is inaccessible from the bulk-based or *ex situ* techniques, being a unique tool to probe solid-state phase transitions in alkali-metal battery systems.[8,18−23]

We find that sodium-ion insertion into MoS$_2$ nanosheets occurs *via* a two-phase reaction mechanism initiated by the nucleation of a new phase NaMoS$_2$ and followed by a propagation of the phase boundary with a velocity of ~3−7 nm/s, which is much smaller than that of lithiation (~30−70 nm/s) reported in the literature.[8] The Na-ion transport within the interlayers of MoS$_2$ fractures the continuous layered structure

into a few nanometer-sized domains *via* formation of crystal defects. With intercalated Na, MoS$_2$ undergoes a phase transition from the 2H to a series of super-structured 1T (NaMoS$_2$) phases, forming tiny domains with a typical size of ~3−5 nm. The lattice expansion caused by insertion of Na is small as the strain is almost relaxed due to the introduction of high-density defects. These observations provide useful insights into understanding the mechanism of MoS$_2$-based batteries and the coupling between structure and (both electrical and ionic) transport properties of the layered two-dimensional MoS$_2$ material.

RESULTS AND DISCUSSION

The pristine MoS$_2$ nanosheet used for this study has a trigonal prismatic (2H) structure, as shown in Figure 1a (JSPDS02-0132; a = 0.315 nm; c = 1.23 nm). A solid battery cell, consisting of a very thin sheet of MoS$_2$ and Na counter electrode, was fabricated to work inside the TEM chamber (Figure 1b; see also Supporting Information Figure S1). The edge of the nanosheet was usually slightly curved, and therefore, the (001) planes were also visible at the edge. Figure 1c shows a typical MoS$_2$ nanosheet with a thickness of ~5 unit cells (equivalent to ~6 nm). In the pristine MoS$_2$ nanosheet, the (001) planes were parallel to each other and the layer distance was 0.615 nm. After Na intercalation in Figure 1d, the layered structure of NaMoS$_2$ was broken into tiny "nanodomains" with a typical size of ~5 nm separated by the "cracks". Only within these
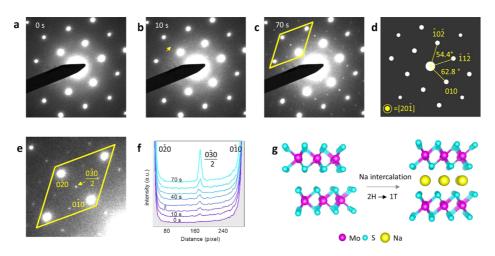
Figure 2. Structural evolution during sodium intercalation. (a) Electron diffraction pattern of the pristine single-crystal MoS_2 nanosheet. (b) Upon sodium intercalation, superstructure diffraction spots appear. (c) With further Na intercalation, the superstructure spots become intense. (d) Simulated electron diffraction pattern of the $2H$-MoS_2 phase with the electron beam direction of $[20\bar{1}]$, which matches experimental observation. (e) Enlarged view of electron diffraction pattern from (c), suggesting that the superstructure reflections correspond to a structure of 2×2 $2H$-MoS_2. (f) Line profiles showing the intensity evolution of the superstructure reflection. (g) Atomistic illustration showing that Na intercalation induces phase transition from $2H$-MoS_2 to $1T$-$NaMoS_2$. The viewing direction is $[100]$.

nanodomains were the (001) planes parallel to each other. The mean values of the measured interlayer distance in Figure 1e indicate a small lattice expansion ($\sim$1.0%) in the Na-intercalated MoS_2. Such subtle change in lattice was likely due to the formation of cracks, with which the Na-intercalation-induced strain has been effectively relaxed.

The consecutive selected area electron diffraction (SAED) patterns were recorded to monitor the overall structural evolution upon Na intercalation (Figure 2a–c). The reflections at the pristine state (Figure 2a) can be indexed to $2H$-MoS_2 seen along the $[20\bar{1}]$ direction, which was confirmed by the electron diffraction simulation shown in Figure 2d (see also Figure S2). Similar to other alkali-metal ions, the Na also prefers to occupy the sulfide octahedral sites that have the lowest energy to form $NaMoS_2$.[24] Indeed, the Na ions occupying the S octahedral sites were also directly observed from the scanning TEM.[15] Although accommodation of more Na was also possible before the conversion reaction took place (up to 1.5 Na per MoS_2), in such a case, the layered structure can no longer be fully recovered during deintercalation.[15]

After a few seconds, superstructure reflections start to appear during sodium intercalation (Figure 2b) and gradually become intense (Figure 2c). These superstructure reflections can be indexed as a 2×2 structure of $2H$-MoS_2 (Figure 2e). Upon alkali-metal intercalation in MoS_2, a phase transition from 2H to 1T involving a transversal gliding of one of the S planes was proposed a few decades ago[12,25] (schematically illustrated in Figure 2f), and was confirmed by the electron diffraction[26,27] in $1T$-$LiMoS_2$ and $1T$-$KMoS_2$ systems.[8] However, our simulation indicates that an ideal $1T$-$NaMoS_2$ phase has the same electron diffraction pattern as that with the 2H phase without any superstructure reflections, suggesting that these superstructure reflections are not from a simple 1T configuration of Na intercalated in MoS_2. Although ordering of alkali-metal ions in the intercalated phase might cause a similar electron diffraction pattern, previous studies suggested that such superstructure reflections result from the formation of distorted $1T$-MoS_2 phases.[26] Moreover, the measured in-layer lattice expansion is even subtler than that in the interlayer, which is consistent with previous XRD results.[15]

The Na transport in MoS_2 and phase boundary motion can be tracked in real-time in Figure 3a. The two-phase reaction is in agreement with a previous XRD study.[15] In the $NaMoS_2$ domain, the fast Fourier transform (FFT) pattern also shows a 2×2 superstructure that is consistent with the electron diffraction patterns above. In the high-resolution TEM image, the superstructure lattice stripes in the Na-intercalated domain ($NaMoS_2$) have doubled the space of pristine MoS_2. An enlarged view of phase boundary in Figure 3b that is filtered in the Fourier space by removing the noise signal shows that the measured width of the phase boundary is $\sim$2 nm. Similar phase boundary between 2H- and $1T$-MoS_2 has been proposed as an intermediate phase with distorted lattice,[28] and as a result, a larger strain gradient exists across the phase boundary. This explains that the contrast of the boundary in Figure 3b is different (darker) in the filtered high-resolution phase-contrast TEM image. The area of the Na-intercalated domain is plotted as a function of time to estimate the Na migration rate and boundary velocity. The measured reaction rate of $\sim$3–7 nm/s (10–50 nm^2/s) is much slower than that of lithium diffusion at $\sim$30–70 nm/s[8] (see also Figure S3). The sluggish kinetics for sodium intercalation is likely due to a larger radius (0.116 nm
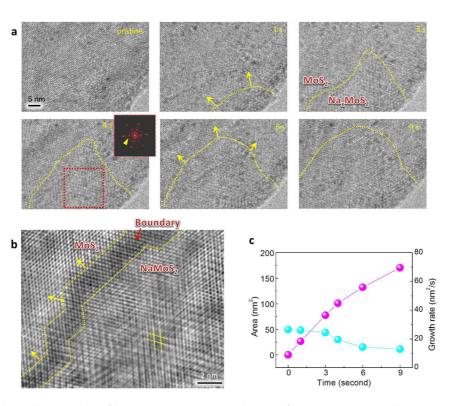
Figure 3. High-resolution tracking of the Na transport in MoS$_2$ and reaction front propagation in real-time. (a) Selected high-resolution TEM image series showing the propagation of the phase boundary of NaMoS$_2$/MoS$_2$. The dashed yellow lines roughly highlight the phase boundary as a guide for the eye. The arrows show the boundary propagation direction. At 4 s, the inset shows a FFT pattern from the NaMoS$_2$ phase. The arrowhead is highlighting the superstructure reflection that agrees with the electron diffraction pattern. **(b)** Enlarged view of the phase boundary at 4 s. The image is filtered in Fourier space using a mask to select the primary lattice and superlattice frequencies and to remove the high-frequency noise above the information transfer limit. **(c)** Area of the sodium-intercalated domain and growth rate (change in domain area with time) are plotted as a function of time.

for Na$^+$ and 0.076 nm for Li$^+$ in ref 29) and heavier mass for Na compared to that for Li, thus slowing down the ionic transport within MoS$_2$.

Figure 4a is recorded from a 1T-NaMoS$_2$ domain with a thickness of ~6 nm (see Figure S4). The superstructure in this region is not uniform even at nanometer scale. Even though the FFT pattern from this selected area also displays a 2 × 2 superstructure (Figure 4a), various nanosized domains with different stripe patterns are distinguishable in Figure 4b. These superstructured domains can be indexed to simple 2 × 1 (or orthorhombic $\sqrt{3}$ × 1 indexes; see also Figure S5), "twinned", or "triplet" superstructures, indicating that 2 × 1 (or orthorhombic $\sqrt{3}$ × 1) superstructure is the elementary cell.[26] Indeed, a previous scanning tunneling microscopy study[30] of restacked MoS$_2$ confirmed that only the 2 × 1 superstructure is observed at the surface, and the electron diffraction pattern from the extremely thin region[26] also suggested a simple 2 × 1 superstructure. In our study, the observed overall 2 × 2 superstructure pattern is likely because both FFT and electron diffraction include a relative large region containing multidomains, and some of these domains overlapped with each other along the electron beam direction. The spatial distribution of these three elementary superstructure domains with different

orientation superstructure can be extracted by inversing the corresponding FFT lattice plane frequencies, as shown in Figure 4c–e. Figure 4f is the color mapping of three elementary superstructures. The typical size of each domain is ~3–5 nm, and the spatial distribution is not uniform.

Now we can compare the sodium intercalation with lithium insertion in the literature.[8] Similar to Li, Na ions can also be intercalated and diffuse in MoS$_2$ to form NaMoS$_2$. After Na insertion, although the layered structure remains, Na insertion causes many defects and breaks the layers into small segments with a typical size less than 5 nm. No significant lattice expansion is observed during Na intercalation, probably because the strain is largely relaxed *via* the introduction of a high density of "crack" defects. Both Na- and Li-ion intercalation can trigger a phase transition from 2H-MoS$_2$ to 1T-NaMoS$_2$ (LiMoS$_2$) as the simulation[31,32] has suggested that the intercalation of Li or Na in MoS$_2$ can effectively reduce the energy of phase transition from 2H to 1T, that is, reduction of 0.59 eV for Li intercalation and 0.34 eV for Na intercalation.[33] Remarkably, the size of distorted 1T-NaMoS$_2$ domains is ~3–5 nm, which is not observed in the distorted 1T-LiMoS$_2$ domains in the literature.[8] During Na diffusion, a velocity of the phase boundary is ~3–7 nm/s,
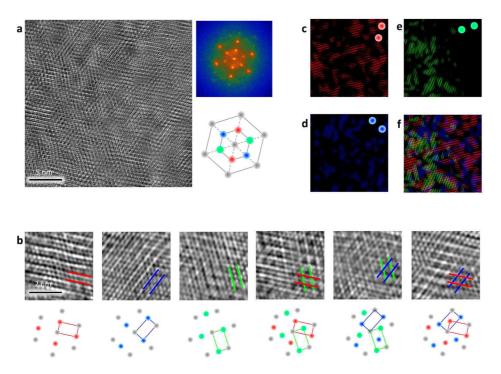
Figure 4. Superstructures in the NaMoS$_2$. (a) High-resolution TEM image of a sodium-intercalated region. The right insets are the corresponding FFT pattern and schematic illustration of reflection spots. The primary lattice frequencies are labeled with gray, and the superlattice frequencies are in red, blue, and green for three different orientations. **(b)** Various nanosized domains are distinguishable in the sodium-intercalated phase. The superstructure stripes show different orientations. The schematics below show the corresponding superstructure reflections (see also Figure S5). The same TEM image is filtered in Fourier space using a mask to select only frequencies in **(c)** red, **(d)** blue, and **(e)** green. These maps show the spatial distribution of the superstructure domains. **(f)** Color mapping of three types of superstructures, indicating inhomogeneous distribution.

which is much slower compared to lithium diffusion at $\sim30-70$ nm/s.[8] The sluggish kinetics for sodium intercalation is likely due to a larger radius[29] and heavier mass for Na compared to Li. The observed distinct kinetics between Li and Na agree well with the first-principle calculations from which the barrier for Li and Na diffusion between adjacent octahedral sites is ~0.49 eV[34] and ~0.7 eV,[24] respectively.

CONCLUSIONS

In summary, we find that Na-ion insertion into MoS$_2$ nanosheets occurs *via* a two-phase reaction initiated by nucleation of a new phase of NaMoS$_2$ and followed by propagation of the phase boundary. The typical width of the phase boundary is ~2 nm, and typical velocity of the phase boundary is $\sim3-7$ nm/s, which is 1 order slower than Li diffusion. The Na-ion diffusion within the interlayers can fracture the continuous layered structure into a few nanometer-sized domains

via formation of high-density defects to relax the strain. Meanwhile, the sodium intercalation triggers a phase transition from 2H-MoS$_2$ to superstructured 1T-NaMoS$_2$ phases with the ordering of lattice distortion. The typical size of tiny superstructured domains is $\sim3-5$ nm. Our direct observations reveal the details of Na-ion intercalation-induced solid-state phase transformation. The similarities and differences between the Na and Li diffusion dynamics in the same material provide useful information to find suitable electrode materials for NIBs. Uncovering the coupling of structure, chemical dopants, and electronic states of MoS$_2$ also deepens our understanding of the fundamental physics in these 2D transition metal dichalcogenides. Moreover, the capability of tracking ion transport in solids at atomic-scale spatial and subsecond temporal resolutions provides unprecedented opportunities to study the dynamics of solid-state phase transformations.

METHODS

To monitor the structural evolution during Na insertion, MoS$_2$ nanosheets with a thickness of a few nanometers were peeled off from a single-crystal MoS$_2$. A solid battery cell consists of a very thin sheet of MoS$_2$ and Na counter electrode. The dynamic process of Na-ion intercalation in MoS$_2$ nanosheets was recorded with subsecond temporal and lattice-fringe spatial

resolution. MoS$_2$ adapts alkali-metal ions between two sulfide layers due to the nature of the negative charge. The sodiation is controlled at the stage of intercalation reaction rather than conversion, within which the MoS$_2$ showed high capacity, excellent rate, and long cycling life.[35] The distance is measured from multiple spots where the lattice is relatively well-reserved. The mean values of pristine and sodium-intercalated phases are

used to estimate the lattice change. The mean value of the pristine state has been normalized to the $c/2 = 0.615$ nm.

Conflict of Interest: The authors declare no competing financial interest.

REFERENCES AND NOTES

1. Whittingham, M. S. Lithium Batteries and Cathode Materials. *Chem. Rev.* **2004**, *104*, 4271–4301.
2. Armand, M.; Tarascon, J. M. Building Better Batteries. *Nature* **2008**, *451*, 652–657.
3. Goodenough, J. B.; Kim, Y. Challenges for Rechargeable Li Batteries. *Chem. Mater.* **2010**, *22*, 587–603.
4. Dunn, B.; Kamath, H.; Tarascon, J.-M. Electrical Energy Storage for the Grid: A Battery of Choices. *Science* **2011**, *334*, 928–935.
5. Doeff, M. M.; Ma, Y. P.; Visco, S. J.; Dejonghe, L. C. Electrochemical Insertion of Sodium into Carbon. *J. Electrochem. Soc.* **1993**, *140*, L169–L170.
6. Liang, Y.; Yoo, H. D.; Li, Y.; Shuai, J.; Calderon, H. A.; Hernandez, F. C. R.; Grabow, L. C.; Yao, Y. Interlayer-Expanded Molybdenum Disulfide Nanocomposites for Electrochemical Magnesium Storage. *Nano Lett.* **2015**, *15*, 2194–2202.
7. Somoano, R. B.; Hadek, V.; Rembaum, A. Alkali-Metal Intercalates of Molybdenum Disulfide. *J. Chem. Phys.* **1973**, *58*, 697–701.
8. Wang, L.; Xu, Z.; Wang, W.; Bai, X. Atomic Mechanism of Dynamic Electrochemical Lithiation Processes of MoS_2 Nanosheets. *J. Am. Chem. Soc.* **2014**, *136*, 6693–6697.
9. Wang, Y.-X.; Seng, K. H.; Chou, S.-L.; Wang, J.-Z.; Guo, Z.; Wexler, D.; Liu, H.-K.; Dou, S.-X. Reversible Sodium Storage *via* Conversion Reaction of a MoS_2-C Composite. *Chem. Commun.* **2014**, *50*, 10730–10733.
10. David, L.; Bhandavat, R.; Singh, G. MoS_2/Graphene Composite Paper for Sodium-Ion Battery Electrodes. *ACS Nano* **2014**, *8*, 1759–1770.
11. Wang, J.; Luo, C.; Gao, T.; Langrock, A.; Mignerey, A. C.; Wang, C. An Advanced MoS_2/Carbon Anode for High-Performance Sodium-Ion Batteries. *Small* **2015**, *11*, 473–481.
12. Mattheiss, L. F. Band Structures of Transition-Metal-Dichalcogenide Layer Comoounds. *Phys. Rev. B* **1973**, *8*, 3719–3740.
13. Wypych, F.; Schollhorn, R. 1T-MOS₂, A New Metallic Modification of Molybdenum-Disulfide. *J. Chem. Soc., Chem. Commun.* **1992**, *19*, 1386–1388.
14. Bissessur, R.; Kanatzidis, M. G.; Schindler, J. L.; Kannewurf, C. R. Encapsulation of Polymers into MoS_2 and Metal to Insulator Transition in Metastable MoS_2. *J. Chem. Soc., Chem. Commun.* **1993**, *20*, 1582–1585.
15. Wang, X.; Shen, X.; Wang, Z.; Yu, R.; Chen, L. Atomic-Scale Clarification of Structural Transition of MoS_2 upon Sodium Intercalation. *ACS Nano* **2014**, *8*, 11394–11400.
16. Gao, P.; Kang, Z.; Fu, W.; Wang, W.; Bai, X.; Wang, E. Electrically Driven Redox Process in Cerium Oxides. *J. Am. Chem. Soc.* **2010**, *132*, 4197–4201.
17. Gao, P.; Nelson, C. T.; Jokisaari, J. R.; Baek, S.-H.; Bark, C. W.; Zhang, Y.; Wang, E.; Schlom, D. G.; Eom, C.-B.; Pan, X. Revealing the Roles of Defects in Ferroelectric Switching with Atomic Resolution. *Nat. Commun.* **2011**, *2*, 591.
18. Huang, J. Y.; Zhong, L.; Wang, C. M.; Sullivan, J. P.; Xu, W.; Zhang, L. Q.; Mao, S. X.; Hudak, N. S.; Liu, X. H.; Subramanian, A.; et al. *In Situ* Observation of the Electrochemical Lithiation of a Single SnO_2 Nanowire Electrode. *Science* **2010**, *330*, 1515–1520.
19. Liu, X. H.; Wang, J. W.; Huang, S.; Fan, F. F.; Huang, X.; Liu, Y.; Krylyuk, S.; Yoo, J.; Dayeh, S. A.; Davydov, A. V.; et al. *In Situ* Atomic-Scale Imaging of Electrochemical Lithiation in Silicon. *Nat. Nanotechnol.* **2012**, *7*, 749–756.
20. Zhu, Y.; Wang, J. W.; Liu, Y.; Liu, X.; Kushima, A.; Liu, Y.; Xu, Y.; Mao, S. X.; Li, J.; Wang, C.; et al. *In Situ* Atomic-Scale Imaging of Phase Boundary Migration in $FePO_4$ Microparticles During Electrochemical Lithiation. *Adv. Mater.* **2013**, *25*, 5461–5466.
21. Niu, J.; Kushima, A.; Qian, X.; Qi, L.; Xiang, K.; Chiang, Y.-M.; Li, J. *In Situ* Observation of Random Solid Solution Zone in $LiFePO_4$ Electrode. *Nano Lett.* **2014**, *14*, 4005–4010.
22. Gu, M.; Li, Y.; Li, X. L.; Hu, S. Y.; Zhang, X. W.; Xu, W.; Thevuthasan, S.; Baer, D. R.; Zhang, J. G.; Liu, J.; Wang, C. M. *In Situ* TEM Study of Lithiation Behavior of Silicon Nanoparticles Attached to and Embedded in a Carbon Matrix. *ACS Nano* **2012**, *6*, 8439–8447.
23. He, K.; Zhou, Y.; Gao, P.; Wang, L.; Pereira, N.; Amatucci, G. G.; Nam, K.-W.; Yang, X.-Q.; Zhu, Y.; Wang, F.; et al. Sodiation *via* Heterogeneous Disproportionation in FeF_2 Electrodes for Sodium-Ion Batteries. *ACS Nano* **2014**, *8*, 7251–7259.
24. Su, J.; Pei, Y.; Yang, Z.; Wang, X. *Ab Initio* Study of Graphene-like Monolayer Molybdenum Disulfide As A Promising Anode Material for Rechargeable Sodium Ion Batteries. *RSC Adv.* **2014**, *4*, 43183–43188.
25. Py, M. A.; Haering, R. R. Structural Sestabilization Induced by Lithium Intercalation in MoS_2 and Related Compounds. *Can. J. Phys.* **1983**, *61*, 76–84.
26. Heising, J.; Kanatzidis, M. G. Structure of Restacked MoS_2 and WS_2 Elucidated by Electron Crystallography. *J. Am. Chem. Soc.* **1999**, *121*, 638–643.
27. Wypych, F.; Solenthaler, C.; Prins, R.; Weber, T. Electron Diffraction Study of Intercalation Compounds Derived from 1T-MoS_2. *J. Solid State Chem.* **1999**, *144*, 430–436.
28. Lin, Y.-C.; Dumcenco, D. O.; Huang, Y.-S.; Suenaga, K. Atomic Mechanism of the Semiconducting-to-Metallic Phase Transition in Single-Layered MoS_2. *Nat. Nanotechnol.* **2014**, *9*, 391–396.
29. Shannon, R. D. Revised Effective Inoic Radii and Systematic Studies of Interatomic Distances in Halides and Chalcogenides. *Acta Crystallogr., Sect. A: Cryst. Phys., Diffr., Theor. Gen. Crystallogr.* **1976**, *32*, 751–767.
30. Qin, X. R.; Yang, D.; Frindt, R. F.; Irwin, J. C. Real-Space Imaging of Single-Layer MoS_2 by Scanning Tunneling Microscopy. *Phys. Rev. B: Condens. Matter Mater. Phys.* **1991**, *44*, 3490–3493.
31. Enyashin, A. N.; Seifert, G. Density-Functional Study of Li_xMoS_2 Intercalates ($0 \leq x \leq 1$). *Comput. Theor. Chem.* **2012**, *999*, 13–20.
32. Esfahani, D. N.; Leenaerts, O.; Sahin, H.; Partoens, B.; Peeters, F. M. Structural Transitions in Monolayer MoS_2 by Lithium Adsorption. *J. Phys. Chem. C* **2015**, *119*, 10602–10609.
33. Gao, G.; Jiao, Y.; Ma, F.; Jiao, Y.; Waclawik, E.; Du, A. Charge Mediated Semiconducting-to-Metallic Phase Transition in Molybdenum Disulfide Monolayer and Hydrogen Evolution Reaction in New 1T' Phase. *J. Phys. Chem. C* **2015**, *119*, 13124–13128.
34. Li, Y.; Wu, D.; Zhou, Z.; Cabrera, C. R.; Chen, Z. Enhanced Li Adsorption and Diffusion on MoS_2 Zigzag Nanoribbons by Edge Effects: A Computational Study. *J. Phys. Chem. Lett.* **2012**, *3*, 2221–2227.
35. Hu, Z.; Wang, L.; Zhang, K.; Wang, J.; Cheng, F.; Tao, Z.; Chen, J. MoS_2 Nanoflowers with Expanded Interlayers As High-Performance Anodes for Sodium-Ion Batteries. *Angew. Chem., Int. Ed.* **2014**, *53*, 12794–12798.